

## The influence of external magnetic fields on crack contrast in magnetic steel detected by induction thermography

by P. Jäckel and U. Netzelmann

Fraunhofer Institute for Nondestructive Testing IZFP, Campus E3 1, 66123 Saarbrücken, Germany,  
udo.netzelmann@izfp.fraunhofer.de

### Abstract

Magnetic materials were investigated by induction thermography at induction frequencies of 80 - 300 kHz. The influence of an external magnetic field on the thermal crack contrast was studied. With proper orientation of the external field, the contrast increased by a factor more than three. Numerical simulations of the static and high-frequency magnetic fields and the temperature distribution were performed. Using a stationary induction field and a modulated external field in the frequency range of 0.28 to 36.5 Hz, lock-in thermography was realized, which shows cracks with good contrast. The technique was applied to crack detection in ferritic steel profiles.

### 1. Introduction

Induction thermography has proven to be an attractive technique for detection of surface defects in metallic components [1]. For magnetic steels, it is well known that the high magnetic permeability leads to efficient heating. The skin depth is of the order of 50  $\mu\text{m}$  at induction frequencies of about 100 kHz. In the literature related to induction thermography, there are calculations of the induction field and the resulting temperature distributions as a function of time [2,3]. Magnetic permeability is however usually treated as a scalar quantity. Our previous experiments on artificial surface defects show, that when applying an additional static magnetic field, the thermal crack contrast may significantly increase or decrease, depending on the orientation of the external magnetic field with respect to the crack [4]. In this contribution, this effect is further investigated by modeling, simulation and experiment.

Magnetization of ferromagnetic materials is a complicated process of Bloch wall movements, rotation of the local magnetization vector and flipping of domain orientations. The process is hysteretic and highly nonlinear with respect to externally applied magnetic fields. Therefore, it is hardly accessible to a description by direct solution of Maxwell's equations. Figure 1 shows a typical hysteresis curve with important parameters. For induction thermography without external bias field, the working point will be in the center of the loop or at the remanence field  $B_r$ . With offset external magnetic field, it will be moved up to the saturation region.

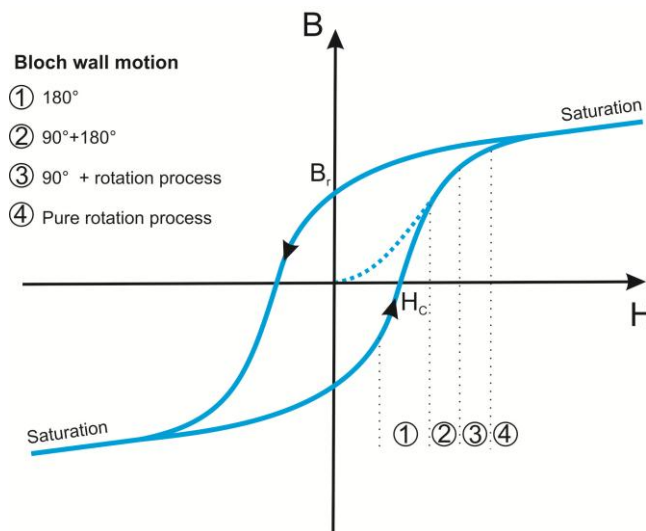


**Fig. 1.** Magnetic hysteresis curve with characteristic parameters

For induction thermography, the power density absorbed in the material when applying a high-frequency alternating magnetic field with frequency  $f$  is of highest importance. In a magnetic material, there are three basic loss

mechanisms: hysteresis losses (proportional to the area of the hysteresis loop), classical eddy current losses (volume currents) and excess losses (eddy currents in the vicinity of active domain walls) [5]. They lead to losses per volume that are proportional to  $f$ ,  $f^2$  and  $f^{3/2}$ , respectively. Usually, for frequencies over 200 Hz, the classical eddy current losses become dominant and the hysteresis curves will change to a more ellipsoidal shape. When the frequency becomes so high that the electromagnetic skin depth  $\delta$  becomes smaller than the dimension of the sample, the frequency dependence will change. This will be discussed in section 3.

## 2. Experimental

Magnetic permeability is a tensor and depends on the external magnetic field and its orientation. It was therefore of interest to study the dependence of the induction signal on these parameters. The combined effect of hysteresis and eddy current losses with superimposed transverse and longitudinal external fields was studied at different excitation field strengths, induction frequencies and field orientations with respect to artificial cracks. Figure 2 shows typical combinations of the directions of the high-frequency and static magnetic fields with respect to a perpendicular surface crack in a sample of a ferromagnetic material.

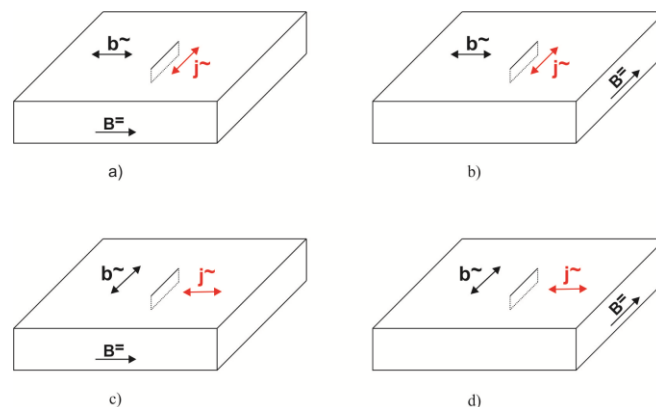


**Fig. 2.** Possible orientations of the dynamic magnetic field  $\tilde{b}$  and the static magnetic field  $\tilde{B}$  with respect to a crack to be detected by induction thermography.  $\tilde{j}$  indicates the main current direction

An experimental set-up as shown in figure 3 was used, implementing the orientation in figure 2a. The sample was mounted between the yokes of an electromagnet, which was driven by a DC current source. The sample made out of ferritic steel had a perpendicular artificial surface crack produced as a notch of 18 mm length, 2.75 mm depth and 0.2 mm width. The sample was positioned in a homogeneous region of the magnetic field. The external field was oriented perpendicular to the crack.

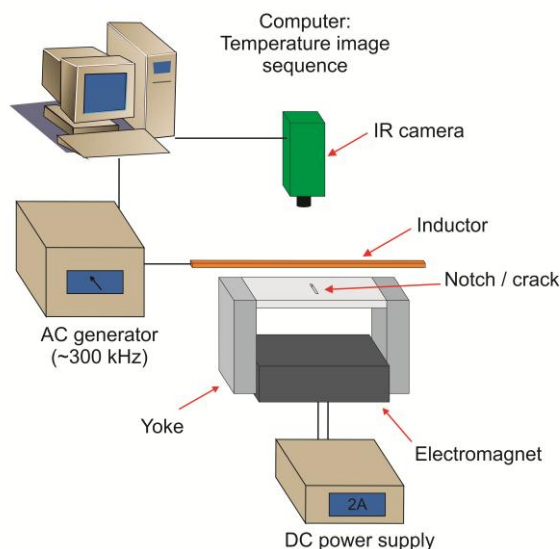


**Fig. 3.** Experimental set-up

Pulsed excitation was realized by an induction generator with maximum power output of 10 kW. Typical excitation frequencies were at 80 to 300 kHz with a typical pulse duration of 300 ms. The MWIR channel (4.4-5.2 μm) of a Thermosensorik QWIP 384 dual-band camera was used for the measurements. Samples were painted black in order to improve and homogenize emission.

The crack contrast in the following is defined as the difference of the peak thermal signal at the crack and the signal background sufficiently far away from the crack at the time of the end of the excitation. In the plot of figure 4, a "relative crack contrast" is shown, where the crack contrast is set to 100% without external field. First, a crack orientation according to figure 2a was studied. In this arrangement, the external magnetic field led to an increase of the relative crack contrast by a factor of more than three (figure 4). A somewhat non-linear behavior of the contrast as a function of the external field is observed. In the orientation of figure 2b, the relative crack contrast decreased with increasing external magnetic field. For the other orientations (figures 2c and d), the external field did show only little effect on the contrast.

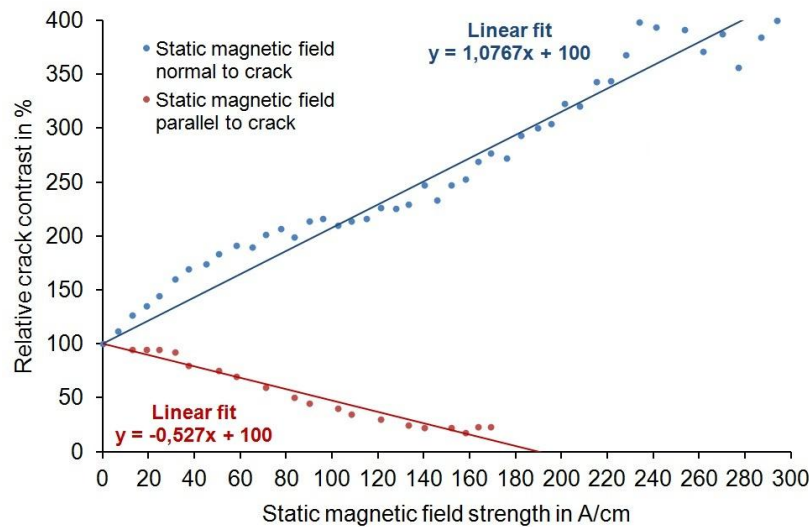


**Fig. 4.** Measured dependence of the relative crack contrast as a function of the external magnetic field in two orientations of the external field

All following examples were studied in an orientation according to figure 2a. A closer look to contrast curves is shown in figure 5, where temperature profiles perpendicular to the center of the crack are plotted at different external magnetic fields.

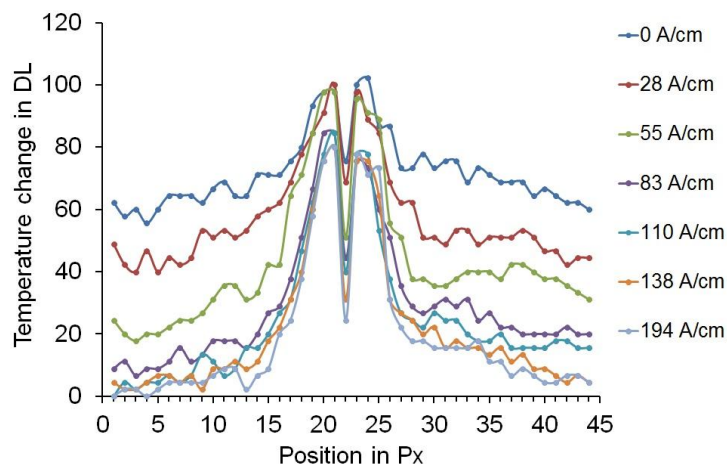


**Fig. 5.** Measured signal profile perpendicular to the crack for various external magnetic fields. An offset was subtracted from all curves (DL = digital levels)

Far away from the crack, a decrease of the surface temperature is observed when a static external magnetic field is applied to the sample. Close to the crack, there is a non-linear behavior of local magnetization and induction

magnetic field. The local power absorption and thereby local heating and temperature decrease less rapidly with the external magnetic field. In total, the result is an increase of the crack contrast with the external field.

Another question was, if the induction high-frequency magnetic field alone would be large enough to cause significant non-linearity even without external magnetic field. The crack signal was studied as a function of the excitation power without external magnetic field. The result is shown in figure 6.

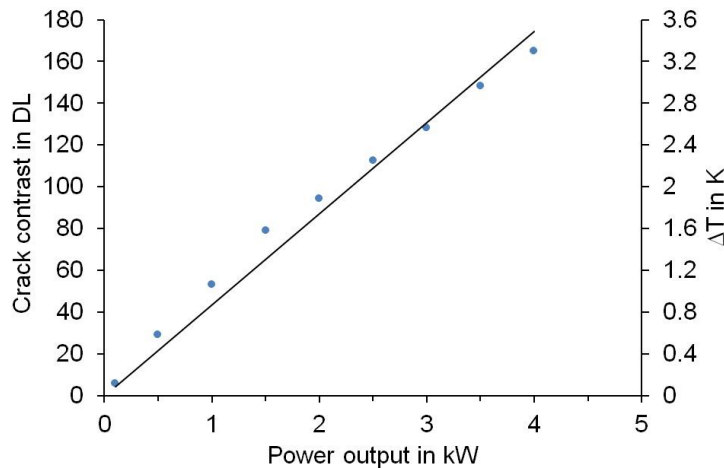


**Fig. 6.** Dependence of the crack contrast of a ferritic steel sample as a function of excitation power at 82.8 kHz without external magnetic field (DL = digital levels)

The dependence is deviating only slightly from linear behavior. This shows, in accordance with estimations based on measured induction currents in the coil and in accordance with simulations, that the main source of non-linearity is caused by the static external field.

### 3. Analytical modelling of heat dissipation

Detailed modeling is limited by the complexity and nonlinearity of the magnetization processes. In the following, the center area of the hysteresis loop is considered. A scalar, linearized analysis for small signal modulation of the magnetic behavior starts with an alternating magnetic field  $H$  and magnetic induction  $B$  of a plane electromagnetic wave:

$$H = H_0 e^{i\omega t}, \quad B = B_0 e^{i(\omega t - \kappa)} \quad (1)$$

Here,  $\kappa$  is a phase factor between magnetic field and induction. From that, the magnetic permeability can be splitted into a real and imaginary part:

$$\mu = \frac{B}{H} = \frac{B_0}{H_0} e^{-i\kappa} = \frac{B_0}{H_0} \cos \kappa - i \frac{B_0}{H_0} \sin \kappa = \mu' - i\mu'' \quad (2)$$

The electromagnetic wave impedance  $Z_0$  describing the ratio of electrical field  $E$  to magnetic field  $H$  of a wave is:

$$Z_0 = \sqrt{\frac{i\omega\mu_0\mu_r}{\sigma + i\omega\varepsilon_0\varepsilon_r}} \quad (3)$$

For steel and the frequencies used in induction thermography, the electrical conductivity  $\sigma$  is so high, that the dielectric term in eq. (3) can be neglected. Then,  $Z_0$  can be written as:

$$Z_0 = \sqrt{\frac{\omega\mu_0}{2\sigma}} (\sqrt{\mu_R} + i\sqrt{\mu_L}) \quad (4)$$

where

$$\mu_R = \sqrt{\mu_r'^2 + \mu_r''^2} + \mu_r'' \quad \text{and} \quad \mu_L = \sqrt{\mu_r'^2 + \mu_r''^2} - \mu_r'' \quad (5)$$

may be denoted as the active and reactive effective magnetic permeability, respectively. The power density is given by the Poynting vector  $\vec{S}$ . Its temporal average is calculated from:

$$\bar{S} = \frac{1}{\mu_0} \frac{1}{2} |\text{Re}(\vec{E} \times \vec{B})| = \frac{1}{2} \frac{1}{\mu_0} B^2 |\text{Re}(Z_0)| \quad (6)$$

The power density  $S$  of an electromagnetic plane wave flowing into the surface of a thick magnetic material where a constant magnetic induction amplitude  $b^-$  is maintained at the surface then behaves as:

$$S = \frac{1}{2\mu_0} b^{-2} \sqrt{\frac{\pi\mu_0\mu_R}{\sigma}} f \quad (7)$$

There is only little information on the complex permeability of steel as a function of frequency. A measurement and a model for the permeability in ferromagnetic steel were presented in [6]. From that model, the initial low frequency permeability drops to 50% or less at induction frequencies of 100 kHz. The general frequency dependence from eq. (7) proportional to  $f^{0.5}$  is only slightly modified by the frequency dependence of the permeability. Experimental verification has to be left for further work.

#### 4. Modelling

##### 4.1. Static magnetic field

The situation is complicated by the fact that the lines of the external magnetic field are superimposed by the demagnetization fields due to the magnetic poles at a crack. This is the basis of magnetic stray flux testing. There are analytical models that allow the representation of the direction of the static fields in the vicinity of a long crack in a material with constant magnetization [7] (figure 7, left). The strong curvature of the field lines at the crack becomes visible. The field lines would be much less curved if the external field was oriented parallel to the crack.

3D numerical calculations of cracks with finite length were performed using COMSOL Multiphysics. The gray values in figure 7, right, represent the absolute of the magnetic flux density. Bright areas represent higher density. The magnetic flux density is significantly increased at the crack tips, but reduced in the center of the crack line.

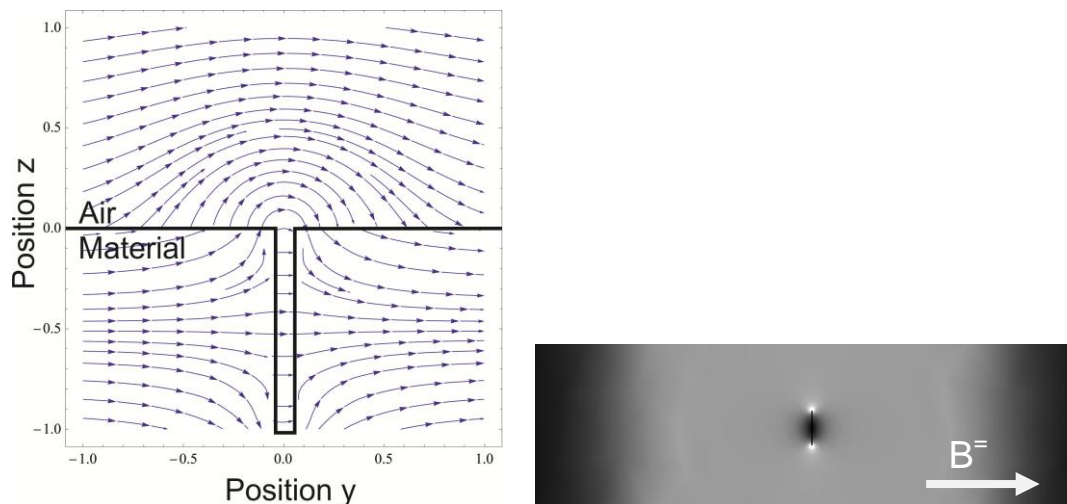


**Fig. 7.** Left: Calculated magnetic induction lines for a body externally magnetized in y-direction with a notch (cross section view). Right: Numerical simulation of the surface magnetic flux density around a crack (sample top view)

##### 4.2. Static and high frequency magnetic field

Calculations with 3D numerical simulation tools were also used to calculate the high frequency magnetic field distribution based on a model of the hysteresis curve of the material, as shown in figure 8. The inductor is crossing the sample in the mid of the crack length.

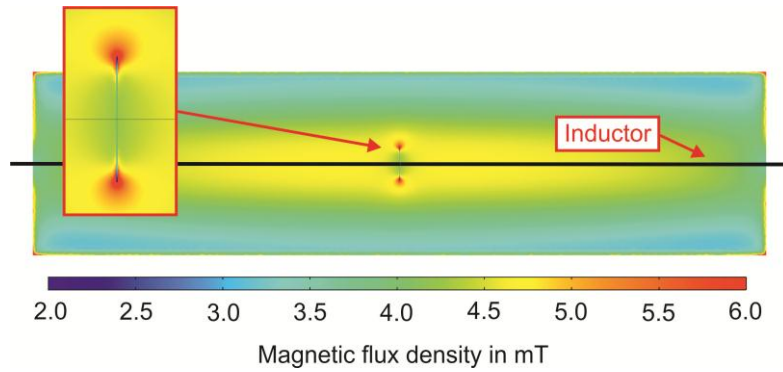


**Fig. 8.** Calculated distribution of the induced high-frequency magnetic flux density (sample top view). The inset shows the crack area in detail

As expected, the magnetic flux is decreasing rapidly with distance from the inductor. Due to the conservation of magnetic flux, a concentration of the high-frequency magnetic field at the crack tips is observed.

The multiphysics simulation finally allows one to compare the calculated thermal distribution with the measured distribution. Both simulated and experimental data were normalized to the a scale from the minimum temperature value in black and the maximum temperature value in white. In figure 9, the comparison between experiment and simulation is shown. In the simulation image, a black horizontal bar was added to locate the position of the inductor. A quite good agreement between simulation and experiment was achieved.

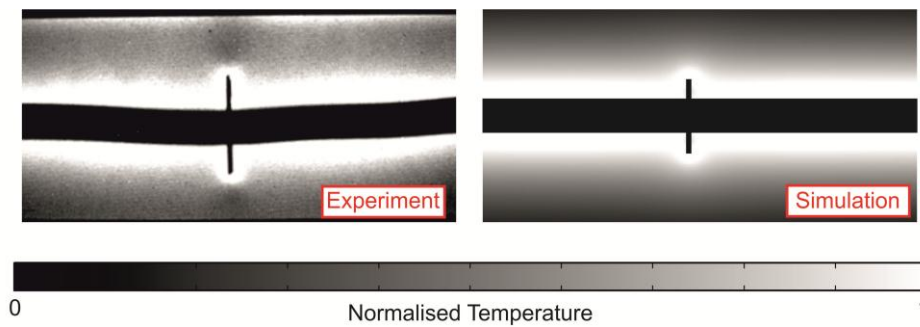


**Fig. 9.** Comparison of experimental data (left) obtained on a sample with artificial crack with simulated data (right). The normalized temperature is shown in grey values.

## 5. External magnetic field modulated induction thermography

The dependence of the thermal signal on the external magnetic field can also be used for an externally magnetic field modulated induction lock-in thermography (EMILT). In this approach, a high frequency induction field is applied with constant amplitude over time. At the same time, an externally applied magnetic field is modulated at low frequencies around 10 Hz. The experimental setup is shown in figure 10.

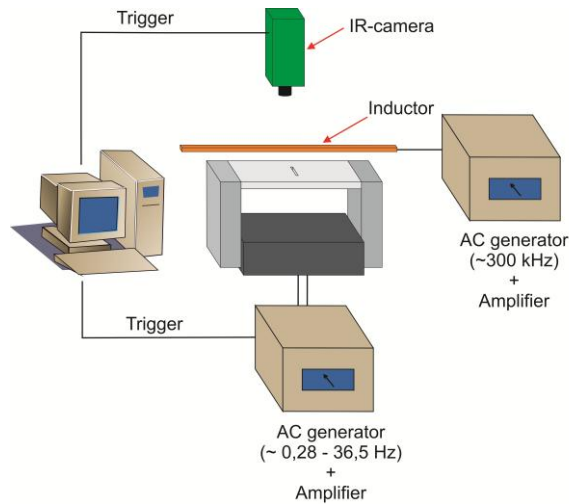


**Fig. 10.** Experimental setup used for externally magnetic field modulated induction lock-in thermography (EMILT)

After switching on the high-frequency field, the surface temperature rise with time (initially proportional to  $t^{0.5}$ ). This is superimposed by oscillations due to the magnet field dependence of the heating effect. These oscillations are analysed after recording many modulation cycles by a usual lock-in thermography algorithm. Amplitude and Phase images will result. They show the crack with particular high contrast. figure 11 shows thermal amplitude profiles perpendicular to a crack at different amplitudes of the external modulation field.

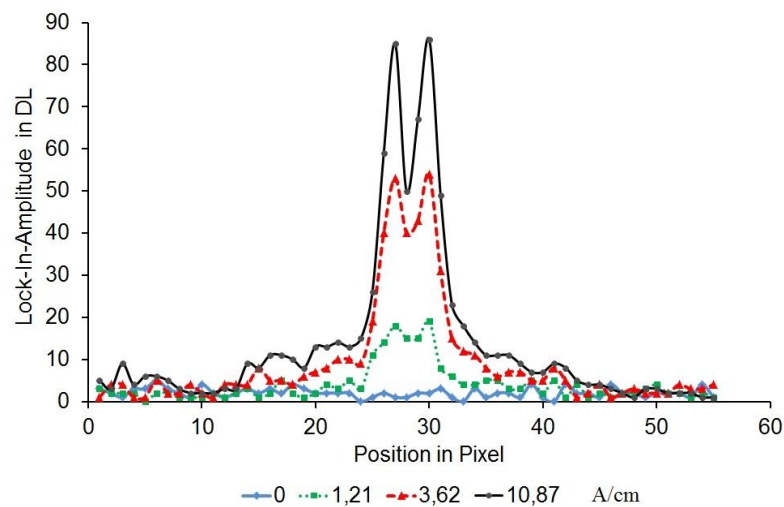


**Fig. 11.** Experimental thermal amplitude profiles over a crack at different external modulation field amplitudes

With increasing modulation field, the crack contrast in the amplitude image is increasing rapidly. Further investigations show, that a saturation effect due to magnetic saturation of the sample occurs, when the field modulation is increased beyond 15 A/cm [8]. It should be noted that the effect of the low frequency static field modulation alone is too weak to generate a measurable heating of the specimen.

## 6. Application

During forming of industrial raw materials, cracks may occur due to different mechanisms. In the following example, a U-profile from ferritic steel was investigated, where a natural crack has occurred which was visible by eye (figure 12). The profile was moved through the yokes of an electromagnet, an induction coil with single loop was used for static magnetization. No surface paint was used. A high-frequency pulse was used for excitation. As expected, the crack generates a strong contrast in the thermographic image. The asymmetric shape of the crack thermal profile indicates that the crack is not perpendicular, but inclined to the surface (figures 12 and 13). In figure 13 it becomes obvious, that the crack contrast is increased by the external magnetic field.

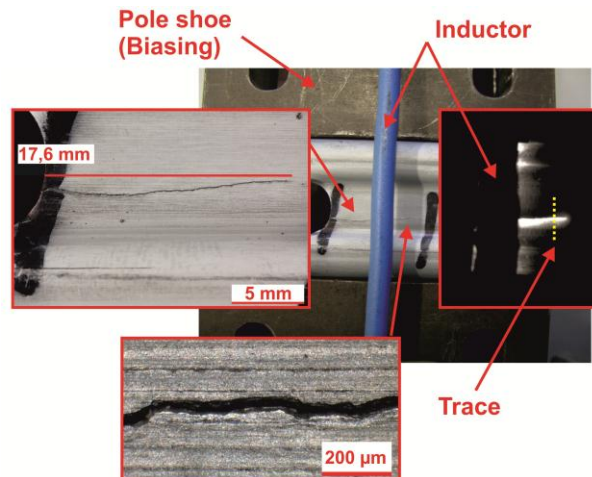


**Fig. 12.** Photos of a natural crack in a ferritic steel profile and a part of the experimental setup. Small inset right: Thermographic image of the crack contrast

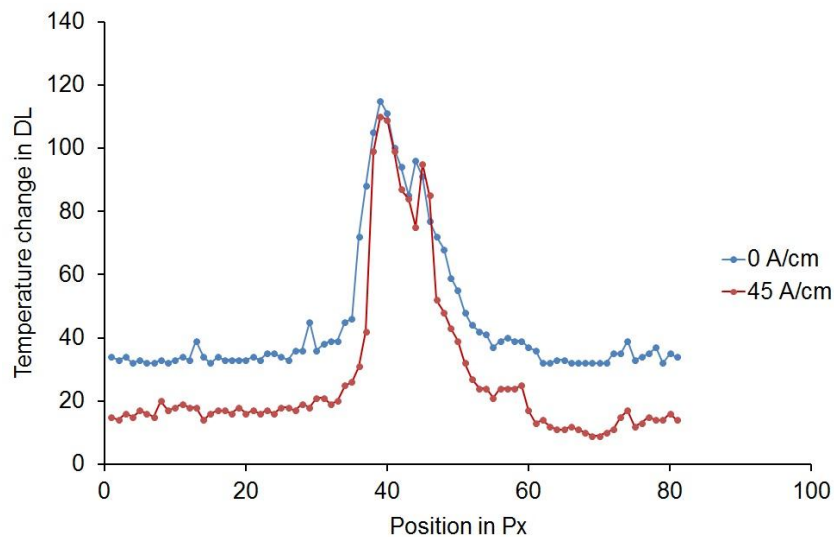


**Fig. 13.** Thermal signal profiles over the crack along the measurement trace shown in figure 12 without and with external magnetic field.

## 7. Summary and conclusion

When performing induction thermography on magnetic steel, the crack contrast can be influenced by applying an external magnetic field. The effect is dependent on the orientation of the external field. For contrast improvement, external field and induction current flow should be applied perpendicular to crack orientation.

The high frequency magnetic fields were usually smaller than the static fields. For a small-signal linearized model, the power absorption during the induction process could be calculated. The static and high-frequency magnetic field distribution were simulated numerically, where a simplified hysteretic behaviour was taken into account. With such a model, the thermal profile could be calculated with good qualitative agreement to the experiment. That does not mean that the relevant processes are understood in detail at present stage. Our present interpretation is based on the fact that the crack is surrounded by areas with changed orientation and density of the magnetic field lines, which influences local high frequency absorption depending on the external field. In a sense, induction thermography is enriched with elements of magnetic stray field testing.

An externally modulated induction lock-in thermography (EMILT) was demonstrated, where the external field was used for an effect modulation. The crack contrast was improved significantly.

First applications demonstrate that the approach is working also on natural cracks. In the future, the technique could be an alternative to magnetic particle testing. The magnetization equipment already present for this technique could be used.

## REFERENCES

- [1] U. Netzelmann and G. Walle, 'Induction Thermography as a Tool for Reliable Detection of Surface Defects in Forged Components', Proc. 17th World Conference on Nondestructive Testing, 25-28 Oct 2008, Shanghai, China
- [2] B. Oswald-Tranta, 'Thermoinductive investigations of magnetic materials for surface cracks', QIRT Journal **1** (2004) 33-46
- [3] J. Vrana, M. Goldammer, J. Baumann, M. Rothenfusser, W. Arnold: 'Mechanisms and Models for Crack Detection with Induction Thermography', Rev. QNDE **27** (2008), D.O. Thompson, D.E. Chimenti (eds), Melville: AIP (2008), 475-482
- [4] H. Strauß, 'Untersuchungen zur Charakterisierung von Oberflächenrissen sowie verdeckten Rissen in ferromagnetischen Materialien mittels einer thermischen Prüftechnik mit induktiver Anregung', Diploma thesis, Universität des Saarlandes und Fraunhofer IZFP, 2007
- [5] G. Bertotti, "Hysteresis in Magnetism", (Academic Press, San Diego 1998)
- [6] N. Bowler, 'Frequency dependence of relative permeability in steel', D. Thompson and D. Chimenti (eds.), Rev. Quant. NDE **25** (2006) 1269-1276
- [7] V. Sherbinin and A. Pashagin, 'Influence of the extension of a defect on the magnitude of its magnetic field', Defectoskopiya **4** (1972), 74-82
- [8] P. Jäckel und U. Netzelmann, 'Erhöhung des Risskontrasts bei der induktiv angeregten Thermographie an ferritischen Stählen durch ein externes Magnetfeld', Thermographie Kolloquium 2011, 29.-30.9.2011, Stuttgart, DGZfP Berichtsband BB 130-CD, V08 (2011)